LATE-TIME OBSERVATIONS OF GRB 080319B: JET BREAK, HOST GALAXY, AND ACCOMPANYING SUPERNOVA

N. R. TANVIR[1], E. ROL[2], A. J. LEVAN[3], K. SVENSSON[3], A. S. FRUCHTER[4], J. GRANOT[5], P. T. O'BRIEN[1], K. WIERSEMA[1],
R. L. C. STARLING[1], P. JAKOBSSON[6], J. FYNBO[7], J. HJORTH[7], P. A. CURRAN[8], A. J. VAN DER HORST[9,13], C. KOUVELIOTOU[9],
J. L. RACUSIN[10], D. N. BURROWS[11], AND F. GENET[12]

[1] Department of Physics and Astronomy, University of Leicester, University Road, Leicester LE1 7RH, UK; nrt3@star.le.ac.uk
[2] Astronomical Institute "Anton Pannekoek," P.O. Box 94248, NL-1090 SJ Amsterdam, The Netherlands
[3] Department of Physics, University of Warwick, Coventry CV4 7AL, UK
[4] Space Telescope Science Institute, 3700 San Martin Drive, Baltimore, MD 21218, USA
[5] Centre for Astrophysics Research, University of Hertfordshire, College Lane, Hatfield AL10 9AB, UK
[6] Centre for Astrophysics and Cosmology, Science Institute, University of Iceland, Dunhagi 5, IS-107 Reykjavik, Iceland
[7] Dark Cosmology Centre, Niels Bohr Institute, University of Copenhagen, Juliane Maries vej 30, DK-2100 Copenhagen, Denmark
[8] AIM, CEA/DSM-CNRS, Irfu/SAP, Centre de Saclay, Bât. 709, F-91191 Gif-sur-Yvette, France
[9] NASA/Marshall Space Flight Center, NSSTC, 320 Sparkman Drive, Huntsville, AL 35805, USA
[10] NASA Goddard Space Flight Center, 8800 Greenbelt Rd., Code 661, Greenbelt, MD 20771, USA
[11] Department of Astronomy and Astrophysics, Pennsylvania State University, 525 Davey Lab, University Park, PA 16802, USA
[12] Racah Institute of Physics, Hebrew University, 91904 Jerusalem, Israel

ABSTRACT

The *Swift*-discovered GRB 080319B was by far the most distant source ever observed at naked-eye brightness, reaching a peak apparent magnitude of 5.3 at a redshift of $z = 0.937$. We present our late-time optical (*Hubble Space Telescope*, Gemini, and Very Large Telescope) and X-ray (*Chandra*) observations, which confirm that an achromatic break occurred in the power-law afterglow light curve at ~ 11 days post-burst. This most likely indicates that the gamma-ray burst (GRB) outflow was collimated, which for a uniform jet would imply a total energy in the jet $E_{\rm jet} \gtrsim 10^{52}$ erg. Our observations also show a late-time excess of red light, which is well explained if the GRB was accompanied by a supernova (SN), similar to those seen in some other long-duration GRBs. The latest observations are dominated by light from the host and show that the GRB took place in a faint dwarf galaxy ($r(AB) \approx 27.0$, rest frame $M_B \approx -17.2$). This galaxy is small even by the standards of other GRB hosts, which is suggestive of a low-metallicity environment. Intriguingly, the properties of this extreme event—a small host and bright SN—are entirely typical of the very low luminosity bursts such as GRB 980425 and GRB 060218.

Key words: galaxies: high-redshift – gamma-ray burst: individual (GRB 080319B) – supernovae: individual

Online-only material: color figures

1. INTRODUCTION

GRB 080319B was one of the brightest gamma-ray bursts (GRBs) yet seen in gamma rays, and uniquely bright in optical and X-ray wavelengths. At a redshift of $z = 0.937$ (Vreeswijk et al. 2008) this also translates to a record-breaking intrinsic peak luminosity in the optical, being approximately 2 mag brighter than GRB 990123 (Akerlof et al. 1999) and a magnitude brighter than GRB 050904 (Haislip et al. 2006).

By good fortune, an earlier burst, GRB 080319A, had already taken place nearby on the sky roughly 25 minutes before GRB 080319B, so several wide-field optical cameras obtained imaging of the prompt phase, giving unprecedented coverage of the optical flash, and showing it to reach a visual magnitude of 5.3 (Racusin et al. 2008).

Despite (or perhaps because of) the exceptionally dense multi-wavelength coverage of this event and its afterglow, modeling its properties has proven difficult. A number of authors initially argued that the (soft) gamma-ray component was likely dominated by synchrotron self-Compton (SSC), i.e., inverse Compton upscattering of (optical) synchrotron photons that are produced by the same population of relativistic electrons. This was supported by rough similarity of the optical and gamma-ray prompt light curves. If this were the case, then second-order SSC should create another peak of emission in the GeV regime, of

even greater total fluence (Kumar & Panaitescu 2008; Racusin et al. 2008; Piran et al. 2009). This potentially leads to a serious energy crisis, with the total radiated and kinetic energies, if isotropic, being comparable to or even in excess of the rest-mass energy of a massive star.

Subsequent analyses have been unable to construct a consistent SSC model and have argued instead that the two (optical and soft gamma-ray) prompt components must be produced in different regions (Zou et al. 2009) or that they are produced by a relativistically turbulent outflow, rather than internal shocks, at relatively large radius (Kumar & Narayan 2009).

The later time behavior has proven similarly contentious. It has long been thought that GRB outflows are likely to be collimated into narrow jets and that this could reduce the total energy requirement by 1–3 (and in extreme cases perhaps more) orders of magnitude. The observational signature of such beaming is an achromatic break (hereafter referred to as a "jet break") in the power-law decline of afterglow light (Rhoads 1999; Sari et al. 1999). However, the luminosity of GRB 080319B and its afterglow may still stretch plausible models for both the prompt and afterglow emission.

Racusin et al. (2008) proposed a model in which the jet giving rise to the GRB has a particularly high-velocity, bright and narrow ($\sim 0°.2$) core which produces a jet break ~ 1 hr post-burst and dominates the early emission. A wider ($\sim 4°$), more "conventional" jet surrounds this and dominates at intermediate

---

[13] NASA Postdoctoral Program Fellow.

and late times. This second jet is assumed to give rise to the break at $\sim 10^6$ s seen in the *Swift*/XRT light curve.

In a model of this sort, the extreme behavior of the burst is partially explained by the low probability of an observer being within the aperture of the narrow jet. For GRB 080319B, the fraction of observers viewing the gamma-ray emission from the bright and narrow jet would be roughly a factor of 400 lower than those seeing the broad jet. It also provides a reasonably good description of aspects of the temporal evolution of the afterglow. However, the model also requires a further coincidence of a (rarely seen) strong reverse shock from the wider jet creating the early optical afterglow, and this double coincidence seems a less natural scenario. We also note that such an extreme ratio of opening angles and solid angles between the wide- and narrow-jet components is much larger than the ratio of ~ 3 in opening angles expected in the original motivations for the two-component jet models, which include the cocoon in the context of the collapsar model and the neutron decoupling during the acceleration and collimation of a hydromagnetic jet (see Peng et al. 2005, and references therein). Furthermore, the required half-opening angle of the narrow jet ($0°.2$) is extremely small and only slightly above the inverse of the initial Lorentz factor.

An alternative model developed by Racusin et al. (2008) has a single jet, ploughing into a complex density medium. In this case, the evolution of the cooling break frequency is proposed to drive the changes in the broad spectral energy distribution (SED) of the afterglow.

Regardless of the successes and limitations of such models, it is clearly of great interest to investigate the late-time behavior of GRB 080319B and to place it in context with other bursts, which may provide independent clues to its nature. Is the late-time evolution comparable to that seen in most long-duration GRBs? In particular, is the sharp break in the X-ray light curve at $\sim 10^6$ s achromatic, as predicted for a jet break, and what does this imply for the energetics of the burst? Is the burst accompanied by a characteristic Type Ic supernova (SN)? Is the underlying host galaxy similar to those of other long-duration GRBs?

In this paper, we describe our late-time optical and X-ray monitoring of the transient and host galaxy emission of GRB 080319B, utilizing Gemini-North, *Hubble Space Telescope* (*HST*), the Very Large Telescope (VLT), and *Chandra*.

2. OBSERVATIONS AND REDUCTION

2.1. X-ray Observations

In order to follow the X-ray light curve out to late times, beyond the sensitivity limit of the *Swift*/XRT, we obtained observations with *Chandra*/ACIS (S3 chip), roughly 38 and 58 days after the burst. We used the standard processed data (ASCDS version 7.6.11.6) for our analysis, selecting an energy range between 0.3 and 7 keV, which gave an optimal signal to noise. Photometry was performed with a 5 pixel (2.5 arcsec) radius region centered at the source position, and an annular region centered around the source as the background region (inner radius 14 arcsec, outer radius 28 arcsec).

The first epoch consisted of a 9 ks exposure, with 9 counts detected in the source region and a predicted background of 0.4 counts. The second epoch was a 36 ks exposure, resulting in 18 counts in the source region and a 1.48 count background. Data were fitted inside XSpec using appropriate response matrices, with the actual fitted values for photon index and absorption from the *Swift*/XRT late-time data (Racusin et al. 2008); thus,

only the normalization was fitted. The fluxes were then derived using this normalized fit in the 0.3–10 keV range, giving absorption-corrected values of $8.4^{+3.2}_{-2.7} \times 10^{-15}$ erg cm^{-2} s^{-1} and $3.7^{+1.0}_{-0.8} \times 10^{-15}$ erg cm^{-2} s^{-1} for epochs 1 and 2, respectively. Here, the 1σ errors were derived using Bayesian confidence limit estimation (Kraft et al. 1991).

2.2. Optical/Near-IR Observations

Due largely to its brightness, early optical and near-infrared (nIR) observations of GRB 080319B were pursued by several groups, resulting in a very well sampled optical/nIR light curve covering the first few hours after the burst (Racusin et al. 2008; Bloom et al. 2009; Wozniak et al. 2009; Pandey et al. 2009). Despite its initial brightness, the afterglow faded rapidly, and photometric monitoring required large-aperture telescopes after a few days.

A log of all our late-time observations is provided in Table 1. This does not include any correction for dust extinction: the foreground extinction is expected to be small ($A_V = 0.037$; Schlegel et al. 1998) while the extinction internal to the host, although rather uncertain due to the presence of a break between the optical and X-ray, is also found to be modest (Racusin et al. 2008).

We obtained optical observations with Gemini-North/GMOS, VLT/FORS1, and *HST*/WFPC2 between ~ 3 and ~ 460 days post-burst. Processing of ground-based observations was performed using standard IRAF routines. In particular, the GMOS reduction made use of the relevant customized software provided by Gemini. Photometric calibrations, both zero-point and color terms, were obtained using Sloan Digital Sky Survey (SDSS) stars in the field (Adelman-McCarthy et al. 2007; Cool et al. 2008). For consistency, the FORS1 *B*-band imaging was also calibrated to AB magnitudes.

For our *HST*/WFPC2 observations we placed the target on the WFALL aperture, on the corner of WFC3 closest to the apex, in order to reduce the impact of charge transfer inefficiency (CTE effect), which is significant for the old detectors operating on WFPC2. A four-point dither pattern was used, and subexposures stacked using the DRIZZLE (Fruchter & Hook 2002) software onto a 0.05 arcsec pixel grid (from the native 0.1 arcsec pixels). Photometry of the transient was obtained in a 0.2 arcsec diameter aperture, and aperture corrections to the standard 1 arcsec diameter calculated using brighter point sources on the frame. CTE correction was performed using the method of Dolphin,[14] although we applied only half the correction to the final epoch since the source is clearly extended[15] (extra allowance was made in the error budget for this step). The *HST* photometry was calibrated to AB magnitudes by reference to the tabulated zero points,[16] and then transformed to SDSS *r* and *i* magnitudes for comparison with the ground-based data via the NICMOS Unit Conversion Form.[17]

The position of the afterglow was determined, relative to two well-positioned SDSS stars in the field, to be R.A. = 14:31:40.994, decl. = +36:18:08.64 (J2000), with an error of 0.02 arcsec in each coordinate.[18]

---

[14] http://purcell.as.arizona.edu/wfpc2_calib.

[15] http://www.stsci.edu/hst/wfpc2/documents/isr/wfpc2_isr0004.html.

[16] http://www.stsci.edu/documents/dhb/web/c32_wfpc2dataanal.fm1.html.

[17] http://www.stsci.edu/hst/nicmos/tools/conversion_form.html.

[18] Specifically the comparison stars used from SDSS release 6 were: 587736943056454244 at R.A. = 14:31:41.866, decl. = +36:17:23.13 and 587736943056453784 at R.A. = 14:31:42.912, decl. = +36:18:24.26.

Table 1
Log of the Late-time Observations Reported Here

Time Post-burst (days)	Telescope/camera	Filter	Exposure time (s)	Flux (μJy)	Error	Aperture (diameter arcsec)
3.36	Gemini-N/GMOS	r	5×200	4.33	0.08	2.0
3.38	Gemini-N/GMOS	i	5×200	5.40	0.10	2.0
5.22	Gemini-N/GMOS	r	5×100	2.51	0.09	2.0
5.23	Gemini-N/GMOS	i	5×100	2.91	0.11	2.0
12.3	Gemini-N/GMOS	r	5×100	0.96	0.05	2.0
12.3	Gemini-N/GMOS	i	5×100	1.27	0.07	2.0
26.3[a]	Gemini-N/GMOS	g	6×180	0.174	0.013	1.5
26.3[a]	Gemini-N/GMOS	r	6×180	0.39	0.03	1.5
26.3[a]	Gemini-N/GMOS	i	6×180	0.74	0.03	1.5
27.7[a]	Gemini-N/GMOS	z	6×180	1.09	0.16	1.5
53.2	Gemini-N/GMOS	g	9×300	0.099	0.020	1.5
106.1	Gemini-N/GMOS	g	9×350	0.072	0.007	1.5
319.3	Gemini-N/GMOS	r	10×450	0.062	0.009	1.5
463.1	Gemini-N/GMOS	i	10×360	0.125	0.019	1.5
16.0	VLT/FORS1	B	6×300	0.49	0.08	1.5
25.0	VLT/FORS1	B	6×300	0.24	0.04	1.5
51.0	VLT/FORS2	B	18×300	0.071	0.023	1.5
18.9[b]	*HST*/WFPC2	F606W	8×400	0.55	0.01	0.2
19.1[b]	*HST*/WFPC2	F814W	8×400	0.81	0.02	0.2
53.4[c]	*HST*/WFPC2	F814W	8×400	0.200	0.023	0.2
53.6[c]	*HST*/WFPC2	F606W	8×400	0.066	0.006	0.2
106.4	*HST*/WFPC2	F606W	8×400	0.033	0.009	0.2
				0.065	0.028	1.0
108.3	*HST*/WFPC2	F814W	8×400	0.046	0.027	0.2
				0.219	0.045	1.0

Notes. This photometry is not corrected for extinction, but the small-aperture *HST* photometry has been aperture- and CTE-corrected. Note that these fluxes include both transient light and host light within the apertures, whereas in creating Figure 2 the host contribution was modeled and removed, as described in the text.
[a] Independent reduction of these data already reported in Tanvir et al. (2008b) and Bloom et al. (2009).
[b] Provisional photometry already reported in Tanvir et al. (2008a) and Racusin et al. (2008).
[c] Provisional photometry already reported in Levan et al. (2008).

3. RESULTS

Figure 1 shows the summed *HST*/WFPC2 images at the three epochs of observation. The afterglow luminosity clearly declines with time, being ultimately dominated by light from the host.

Our new X-ray and optical photometry is plotted in Figure 2, together with data from the literature. We expect the optical light curve to consist of three components: the afterglow of the GRB, any accompanying SN, and a steady underlying host galaxy. In the X-ray, the emission is likely to be entirely from the afterglow.

In disentangling these components, our approach is to compare the photometry (corrected for the small foreground Galactic extinction) with a simple, self-consistent model of a power-law afterglow with a sharp achromatic break and an SN. As we will show, this model matches the broad features of the data well and allows us to focus on the main implications of the late-time observations, without getting embroiled in the fine details of the earlier time evolution.

We determine the afterglow power-law slopes solely from the X-ray light curve (adopting the convention flux $F \propto t^{-\alpha} \nu^{-\beta}$), finding $\alpha_1 = 1.28 \pm 0.04$, characteristic of the pre-break decline between 3×10^4 s and 5×10^5 s, and $\alpha_2 = 2.33 \pm 0.37$, characteristic of post-break between 1.2×10^6 s and 4×10^6 s. The break is taken to be abrupt and we find a best fit at 11.6 ± 1.0 days, whilst the spectral slope through the optical bands is taken as $\beta = 0.5$ (Racusin et al. 2008). We note that these values satisfy the closure relations for expansion into a wind-like medium when the cooling break is situated above the optical (Price et al. 2002).

Finally, the SN light curve is based on that of SN1998bw, but faded by 0.3 mag consistent with what is found for several other GRB-SNe (Galama et al. 2000; Zeh et al. 2004). We also include *in the model* a small amount of rest-frame extinction internal to the host of $A_V = 0.06$ (Wozniak et al. 2009) and assume a Pei (1992) Small Magellanic Cloud (SMC) extinction law.

We expect the shorter-wavelength observations (B and g bands) to be largely uncontaminated by SN light, since SNe are weak rest-frame blue and UV emitters due to metal line blanketing. The redder bands therefore constrain any SN component, which should rise to a peak roughly one month post-burst. Finally, our latest time observations are dominated by host galaxy emission. However, as shown below, even at a few hundred days post-burst the photometry is still likely to be contaminated by some residual transient light. To allow for this we adopted an iterative procedure: first assuming the last epoch shows only host, hence using this magnitude to correct the earlier photometry for host contribution, and thus allowing modeling of the transient emission. From this model we can then predict the remaining transient flux which is likely to be still in the latest observation in each band, and hence we can re-estimate the host magnitudes with this contamination removed. The correction is about 10% in g, and only a few percent in r and i, and we have increased the photometric error bars to allow that the contamination could actually range from zero up to this value. It is worth emphasizing that the correction even in g only has a small effect on all but the 50+ day photometric points, and does not change the main conclusions we present.
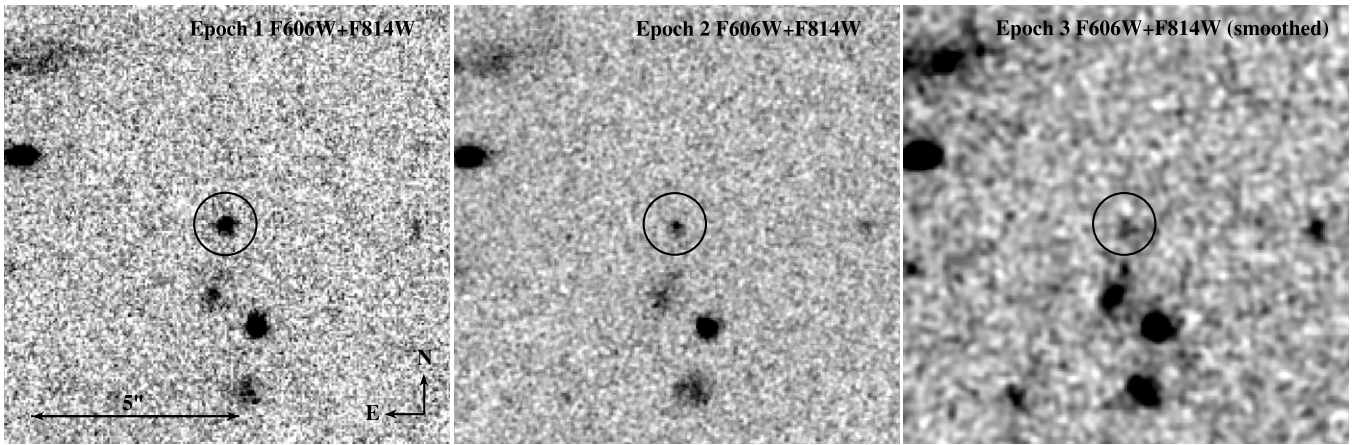
Figure 1. *HST*/WFPC2 images (F606W and F814W combined) at each epoch, as labeled. The circle, whose radius is arbitrary, is centered at the position of the afterglow. The phases are afterglow, SN, and host dominated, respectively. Note that the final panel has been smoothed with a Gaussian kernel to bring out the faint host galaxy light.
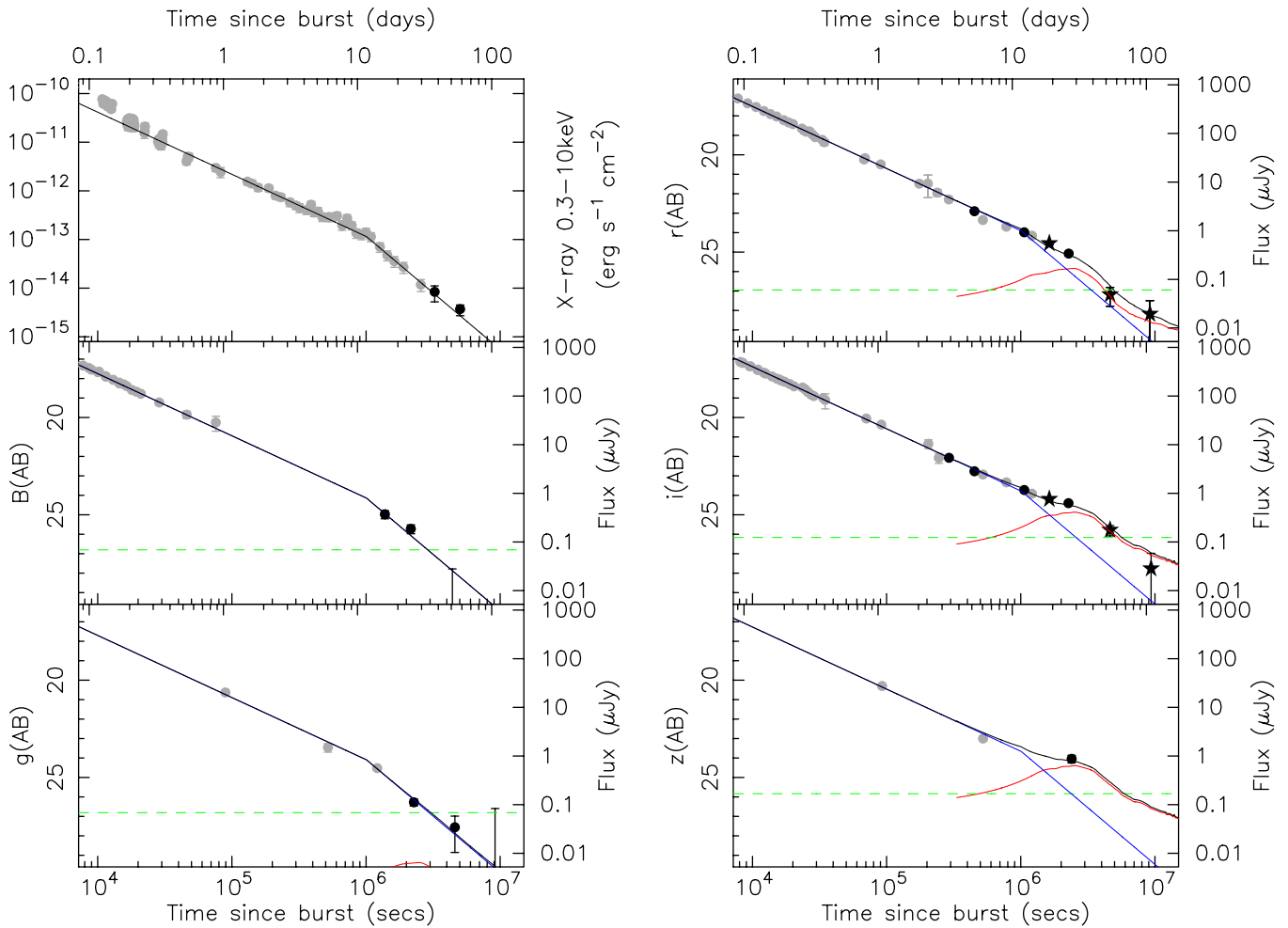

Figure 2. Late-time photometry of GRB 080319B, with bold symbols indicating observations reported here and light symbols being data points from the literature (Racusin et al. 2008; Bloom et al. 2009, and references therein). Photometry has been corrected for foreground extinction, and error bars are 1σ, although in many cases these are smaller than the symbol size. The green dashed lines are the estimated magnitudes of the host galaxy which have been subtracted from the ground-based (filled circles) data. In the case of *HST* images the point-source photometry (filled stars) is done on a scale smaller than the host, and the contribution within the aperture estimated from the latest time images. The blue line is the model afterglow, and the red line is the model SN light curve, as described in the text. The black line is their sum.

(A color version of this figure is available in the online journal.)

For the *HST* observations, since a much smaller aperture can be used, the contribution of host light is less. Here, we make the maximally conservative assumption that 0.5 ± 0.5 of the flux measured in the final *HST* epochs is transient light, and this is then used to correct the earlier epochs for host contamination.

3.1. Jet Break and Energetics

Figure 2 (top left panel) shows our late-time *Chandra* observations, as well as early data taken by the *Swift*/XRT. Our X-ray observations confirm, and increase the confidence in, the break in the X-ray light curve at $t_b \approx 11$ days.

The photometry for the various optical bands, with host contribution subtracted (as described above; see also Section 3.3), is plotted in the other panels of Figure 2. In the *B*- and *g*-band observations, the light curve before and after the break is reasonably consistent with the X-ray slope and break time, indicating approximately achromatic behavior, as expected for a jet break. In fact, this is one of the more convincing examples of a jet break identified in the *Swift* era, when such clear achromatic behavior of X-ray and optical light curves has rarely been seen (e.g., Curran et al. 2008).

Since the jet-break time we find is consistent with that used in earlier studies, notably Racusin et al. (2008) and Bloom et al. (2009), those analyses, and in particular their discussions of deviations from a simple power law at earlier times, are not modified by our findings.

It is instructive to consider the simple case in which the break is interpreted in the context of a single jet (double sided, roughly uniform with reasonably sharp edges). Then a break time, $t_b \approx 11$ days, implies a half-opening angle of $\theta_j \sim 10°$, for a canonical external medium density of $n \sim 1 \text{ cm}^{-3}$ and (an isotropic equivalent) kinetic energy comparable to the energy observed in gamma rays, $E_{k,\text{iso}} \sim E_{\gamma,\text{iso}} = 1.4 \times 10^{54}$ erg (Sari et al. 1999). This, in turn, implies a true energy output in gamma rays within the observed energy range of $E_\gamma \sim 2 \times 10^{52}$ erg, and a comparable kinetic energy in the jet ($E_k \sim E_\gamma$).

Alternatively, the kinetic energy can also be estimated from the X-ray luminosity at 12 hr in the rest frame (Granot et al. 2006; Nousek et al. 2006), from which we find $E_{k,\text{iso}} \approx 7 \times 10^{52}$ erg, for typical microphysical parameters ($\epsilon_e = 0.1$, $\epsilon_B = 0.01$, and $p = 2.2$). This corresponds to $\eta \equiv E_{k,\text{iso}}/E_{\gamma,\text{iso}} \approx 0.05$ and would in turn imply $\theta_j \sim 12°$ and a true kinetic energy of $E_k \sim 2 \times 10^{51}$ erg. The isotropic equivalent kinetic energy at this level would require a very high efficiency of the gamma-ray emission ($\gtrsim 95\%$) for a single wide jet, unless the microphysical parameters were very different so that $E_{k,\text{iso}}$ would be significantly higher. If, on the other hand, the gamma rays were produced by a narrow jet with a considerably higher $E_{k,\text{iso}}$, then this can bring down the efficiency requirements to more reasonable values (Peng et al. 2005). In fact, this feature is built into the two-component jet model of Racusin et al. (2008), which postulates a very narrow ($\theta_{j,n} \sim 0°.2$), very high Lorentz factor ($\Gamma \sim 10^3$) central jet, producing an early break in the light curve, coupled with a wider ($\theta_{j,w} \sim 4°$) jet leading to the later time break we see at $\sim 10^6$ s. This model also mitigates the energy crisis more effectively, with each jet producing $E_\gamma \approx 2 \times 10^{50}$ erg.

Finally, we draw attention to the sharpness of the late-time jet break as seen in the X-rays, which is also consistent with the optical observations, notably in the *g* band. Such a sharp break is not expected for a wind-like external medium (Kumar &

Panaitescu 2000), as considered by Kumar & Panaitescu (2008), and so would require some modification to that simple model, which otherwise nicely fits the afterglow data between $\sim 10^3$ and $\sim 10^6$ s. One possibility would be the coincidental presence of a wind-termination shock in the ambient medium surrounding the progenitor, at approximately the same radius at which the jet break occurs.[19] If we again consider a simple wide jet, this radius is given by $R_j = 1.2 \times 10^{19}(E_k/10^{51})(A_*/0.03)^{-1}$ cm, where $A_* = (\dot{M}/10^{-5}\,M_\odot\,\text{yr}^{-1})/(v/10^8\,\text{cm s}^{-1})$ is the conventional mass-loss scaling (cf. Panaitescu & Kumar 2000). Using the relations $E_k = \eta E_{\gamma,\text{iso}} \theta_j^2/2$ and $\theta_j^2 = [16\pi A c^3 t_b/(1+z)E_{\gamma,\text{iso}}\eta]^{1/2}$ together with the observed values of z, $E_{\gamma,\text{iso}}$, and t_b gives $R_j = 3.1 \times 10^{19}\eta^{1/2}(A_*/0.03)^{-1/2}$ cm. Racusin et al. (2008) argued for a tenuous wind with an upper limit on $A_* < 0.03$ and $\eta \sim 0.07$.

Now, we obtain the wind-termination shock radius using Equation (3) of Pe'er & Wijers (2006): $R_0 = 9.0 \times 10^{17}(A_*/0.03)^{3/10}(v_{w,8}\,t_{*,6})^{2/5}n_{0,3}^{-3/10}$ cm, where $v_{w,8}$ is the wind velocity in units of $10^8\,\text{cm s}^{-1}$, $t_{*,6}$ is the lifetime in units of 10^6 yr of the Wolf–Rayet phase presumed to have driven the wind, and $n_{0,3}$ is the surrounding interstellar matter (ISM) particle density in units of $10^3\,\text{cm}^{-3}$. Hence, the two radii are comparable (around $R \sim 10^{19}$ cm) if, for example, $\eta \sim 0.07$, $A_* = 0.03$, and $n_{0,3}$ has a rather low value ~ 0.0014. If the prompt gamma rays were also produced by this jet then the total energy would be given by $E_{\text{tot}} \approx E_\gamma = E_k/\eta = 9.8 \times 10^{51}(A_*/0.03)^{1/2}(\eta/0.07)^{-1/2}$ erg, comparable to, but somewhat less than, the values found above for a single jet with a uniform external medium of density $n \sim 1\,\text{cm}^{-3}$. If, on the other hand, the gamma rays come from a narrow jet, then E_γ can be much lower, and E_{tot} could be dominated by kinetic energy, $E_k = 6.9 \times 10^{50}(A_*/0.03)^{1/2}(\eta/0.07)^{1/2}$ erg.

3.2. The Supernova

The *r*-, *i*-, and *z*-band observations (Figure 2, right-hand panels) do not show a break at the same time as the bluer bands, but rather exhibit at first a flattening optical decay, and marked reddening, followed by a steepening again after about 40 days. This is illustrated by the change in color of the optical transient from $g - i = 0.60 \pm 0.12$ at 14 days post-burst to $g - i = 1.88 \pm 0.19$ at 26 days. We interpret this as being due to the contribution to the optical light of an underlying SN that begins to dominate the afterglow in the redder bands. Such SN "red humps" have been seen in the light curves of several long-duration GRBs which have been monitored sufficiently deeply at late times (e.g., Galama et al. 2000; Zeh et al. 2004).

As stated above, we follow the conventional procedure of assuming a light curve for the SN component based on that of SN1998bw, which accompanied the low-redshift GRB 980425 (Galama et al. 1998; McKenzie et al. 1999). We redshifted and *k*-corrected these light curves to produce templates in our observed wave bands appropriate to $z = 0.937$, and faded these by 0.3 mag, consistent with the typical GRB-SN "humps" found by Zeh et al. (2004).

When added to the broken power-law afterglow, this produces quite a reasonable match to the photometry of the transient. Thus, we find that GRB 080319B was accompanied by an SN a little fainter than the prototype SN1998bw: an even better match to the photometry would have been achieved with an SN

---

[19] Note that no sharp bump is expected in the light curve when the afterglow shock encounters the wind-termination shock (Nakar & Granot 2007).
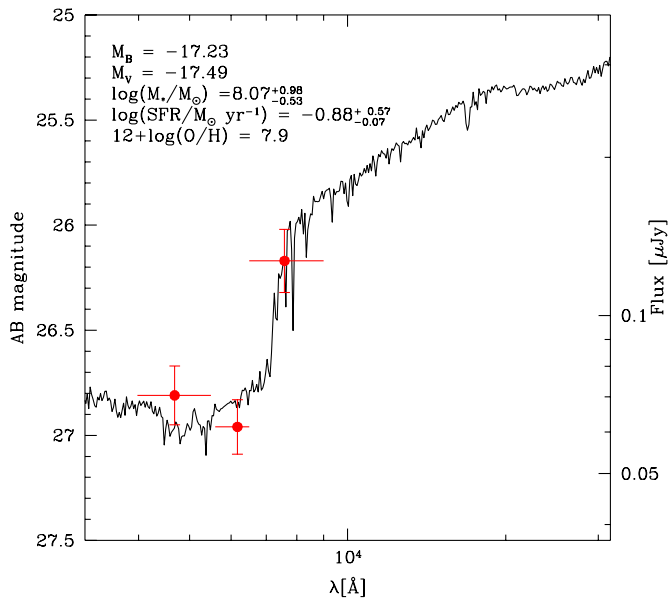
Figure 3. Model spectrum fitted to the three host photometry points. The best-fit model is a young star-forming galaxy (Bruzual & Charlot 2003). Physical parameters are derived from the rest-frame SED: star formation rates (SFRs) are derived from the *U*-band luminosity (Cram et al. 1998); stellar mass is estimated from the *K*-band luminosity with a color correction to the mass-to-light ratio (Mannucci et al. 2005). The χ^2_ν of the fit is a very acceptable 0.89.

(A color version of this figure is available in the online journal.)

Figure 4. Plot of star formation rate vs. stellar mass for a sample of GRB hosts, inferred from template fitting to their photometric SEDs. The host of GRB 080319B, shown by a bold symbol, is at the lower mass and star formation rate end of the distribution. Within the estimated errors, its specific star formation rate seems about average for the sample as a whole. The dashed line shows a locus of constant specific star formation rate, illustrating the typically higher specific SFRs for lower stellar-mass galaxies. The host galaxy sample is that used by Svensson et al. (2010) and includes all GRB hosts with $z < 1.2$, and at least two photometric detections. Parameters determined by SED fits to the photometry, as detailed in the caption to Figure 3. The error bars represent 68% confidence determined by the model fits and illustrate that while neither the stellar mass nor the star-formation rate is tightly constrained by this method, the latter is rather better determined thanks to the detection of flux below the Balmer break, which is dominated by the young stellar component.

model having a peak time a little earlier (a stretch factor < 1 in the language of Zeh et al. 2004). This is in slight disagreement with Bloom et al. (2009) who, using a more preliminary and less complete set of late-time photometry, concluded that an SN component rather brighter than SN1998bw was required.

3.3. The Host Galaxy

Our second-epoch *HST* observations revealed that the afterglow, while still detected, was clearly superimposed upon faint, extended host galaxy emission, with the transient slightly offset north by about 0.2 arcsec from the center of this emission (Levan et al. 2008). By the third epoch the galaxy clearly dominates and is revealed to be a very faint, low surface brightness source extending over roughly 0.5 arcsec. This corresponds to a physical size of about 4 kpc (assuming conventional cosmological parameters) which is quite typical for GRB hosts (Fruchter et al. 2006). The host is not well detected in the WFPC2 images, so the photometry carries a large uncertainty. Our best estimates of the host photometry come from the latest-epoch ground-based imaging, with the *g*-band measurement being corrected to remove the residual transient light by subtracting the flux predicted by our simple model, as described above. Hence, we find (foreground extinction-corrected) host magnitudes of $i(AB) = 26.17 \pm 0.15$, $r(AB) = 26.96 \pm 0.13$, and $g(AB) = 26.81 \pm 0.14$.

This final photometry, while limited, does allow for a crude fit to the galaxy SED. In particular, the relatively blue $g-r$ color (-0.15 ± 0.19), coupled with the red $r-i$ (0.79 ± 0.20), is suggestive of a moderately strong Balmer break, implying the presence of an older stellar population, in addition to the young population which produces the blue rest-frame UV color, and presumably seeded the GRB.

In Figure 3, we show these photometric points fitted with a star-forming galaxy template with the following properties: $M_V = -17.49 \pm 0.15$ and $M_B = -17.23 \pm 0.15$ (quoted errors are statistical). The best fit has an internal extinction $A_V = 0$,
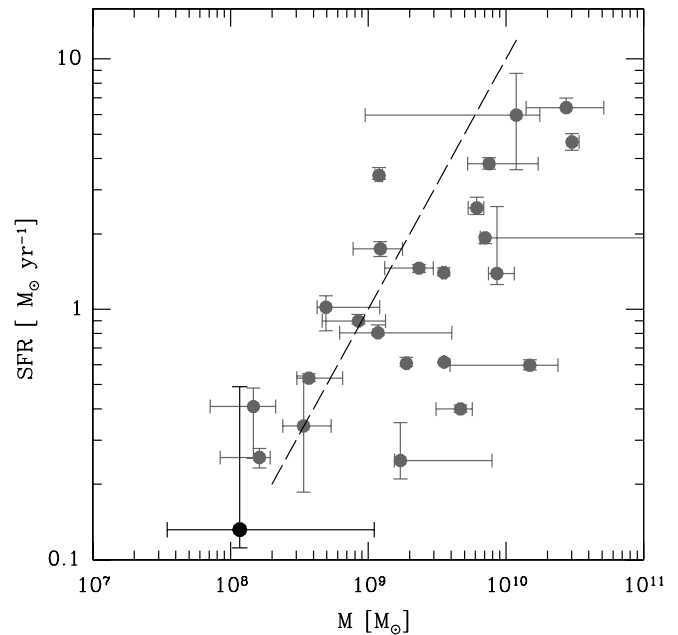
which, although poorly constrained by our limited photometry, is consistent with the low extinction seen to the afterglow. These numbers imply a star formation rate (SFR) $\approx 0.13\ M_\odot\ yr^{-1}$ and stellar mass $M \approx 1.2 \times 10^8\ M_\odot$, although observational and modeling uncertainties make such determinations only accurate to factors of a few. As shown in Figure 4, this indicates that GRB 080319B has one of the smaller hosts found to date, although note that a small number of the faintest GRB hosts, which only have photometric detections in one band, are not included in this figure. The best-fit specific SFR is therefore $\Phi = 1.1\ Gyr^{-1}$ (but with an even greater error bar), which is close to the average for the sample of $z < 1.2$ GRB hosts studied by Svensson et al. (2010).

This luminosity corresponds to about $\frac{1}{40}L_*$ at the observed redshift (cf. Willmer et al. 2006). Such a small galaxy is likely to have low metallicity, although quantifying this is hard, not least because of the small number of data points available for the fit and their large photometric uncertainties. Based on the $z \sim 0.7$ mass–metallicity relationship of Savaglio et al. (2005), the implied metallicity is $12 + \log(O/H) = 7.9$ or about 20% of Solar. However, this numerical value should be treated with caution for various reasons: first, the absolute calibration of the mass–metallicity relation is difficult, and we note that Savaglio et al. (2009), using a revised calibration based on Kewley & Ellison (2008), found metallicities to decrease by ~ 0.5 dex; and second, in the same paper Savaglio et al. (2009) show that GRB hosts with spectroscopically estimated metallicities scatter quite widely around this relation in any case.
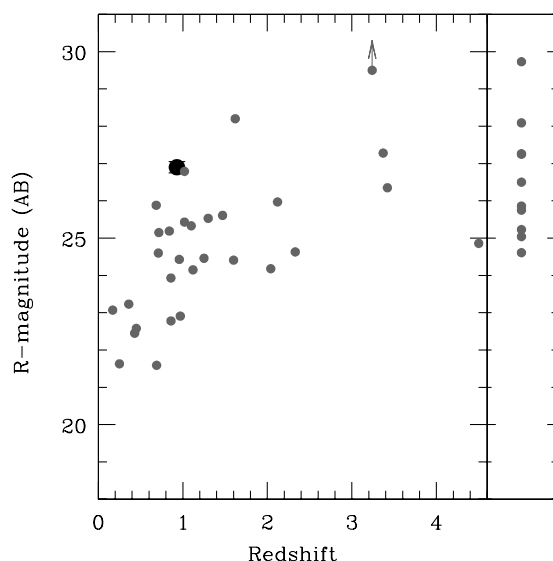
Figure 5. R(AB) magnitude of the host of GRB 080319B compared to a sample of other GRB hosts observed by *HST* as a function of redshift. Those without redshifts are shown in the right-hand panel. Clearly the GRB 080319B host is faint, even by the standards of other GRB hosts.

These properties are within the range of other GRB host galaxies (e.g., Fruchter et al. 2006; Savaglio et al. 2009), but place the GRB 080319B host at the faint end of the available sample. The location of the galaxy in the redshift–magnitude plane is shown in Figure 5, which shows that it is the faintest yet observed by *HST* at comparable redshift. Similarly, the model fit would imply an SFR and stellar mass at the low end, compared to a sample of other GRB hosts (Figure 4). We caution that a proportion of these redshifts were obtained from host rather than afterglow spectroscopy, and hence there is some bias against very faint hosts. For illustration, hosts without redshift are shown in a separate panel on the right side of Figure 5. A particular case in point is that of GRB 980326, which also exhibited an "SN hump" in its light curve suggestive of a redshift $z \sim 1$, but had a host galaxy with $R > 27$ (Bloom et al. 1999).

4. SUMMARY

We have presented a late-time optical and X-ray study of the exceptionally bright GRB 080319B. These data allow us to decompose the contributions from afterglow, SN, and underlying host galaxy. We find that the afterglow of GRB 080319B exhibited an achromatic break in its light curve at $\approx 10^6$ s, which can be interpreted as being due to the relativistic outflow being initially confined within a jet. The sharpness of this break is not expected for a simple R^{-2} wind density profile for the surrounding medium and may indicate that the jet reaches a termination shock in the pre-existing wind at about the same radius, $R \sim 10^{19}$ cm. A simple jet breaking at this time has a total energy $E_{\text{jet}} \gtrsim 10^{52}$ erg. For more complex jet structures in which the gamma ray and late afterglow arise from different components, such as the two-component jet model of Racusin et al. (2008), the total jet energy can be smaller.

In addition GRB 080319B was associated with a bright SN, slightly fainter in luminosity than the prototype SN1998bw. Such SNe, inferred from "red humps" in their light curves, have been found to accompany several other GRBs at similar redshifts (e.g., Zeh et al. 2004). Indeed, apart from the few (generally low-luminosity) bursts with spectroscopically confirmed SN

components, the data set for GRB 080319B provides one of the most compelling examples.

Finally, we have detected a small host galaxy under the position of the GRB, which is fainter than other GRB hosts observed so far at comparable redshifts. This is likely to indicate a low-metallicity environment, and one might speculate that this could be related to the extreme properties of the burst. However, it is also notable that most of the weakest GRBs known (particularly GRB 980425 and GRB 060218) have also occurred in small, low-metallicity hosts and been accompanied by energetic Type Ibc SNe (e.g., Stanek et al. 2006; Wiersema et al. 2007).

REFERENCES

Adelman-McCarthy, J. K., et al. 2007, ApJS, 172, 634
Akerlof, C., et al. 1999, Nature, 398, 400
Bloom, J. S., et al. 1999, Nature, 401, 453
Bloom, J. S., et al. 2009, ApJ, 691, 723
Bruzual, A. G., & Charlot, S. 2003, MNRAS, 344, 1000
Cool, R. J., et al. 2008, GRB Coordinates Network, 7465, 1
Cram, L., Hopkins, A., Mobasher, B., & Rowan-Robinson, M. 1998, ApJ, 507, 155
Curran, P. A., van der Horst, A. J., & Wijers, R. A. M. J. 2008, MNRAS, 386, 859
Fruchter, A. S., & Hook, R. N. 2002, PASP, 114, 144
Fruchter, A. S., et al. 2006, Nature, 441, 463
Galama, T. J., et al. 1998, Nature, 395, 670

Galama, T. J., et al. 2000, ApJ, 536, 185
Granot, J., Königl, A., & Piran, T. 2006, MNRAS, 370, 1946
Haislip, J. B., et al. 2006, Nature, 440, 181
Kewley, L. J., & Ellison, S. L. 2008, ApJ, 681, 1183
Kraft, R. P., Burrows, D. N., & Nousek, J. A. 1991, ApJ, 374, 344
Kumar, P., & Narayan, R. 2009, MNRAS, 395, 472
Kumar, P., & Panaitescu, A. 2000, ApJ, 541, L51
Kumar, P., & Panaitescu, A. 2008, MNRAS, 391, L19
Levan, A. J., Tanvir, N. R., & Fruchter, A. S. 2008, GRB Coordinates Network, 7710, 1
Mannucci, F., Della Valle, M., Panagia, N., Cappellaro, E., Cresci, G., Maiolino, R., Petrosian, A., & Turatto, M. 2005, A&A, 433, 807
McKenzie, E. H., & Schaefer, B. E. 1999, PASP, 111, 964
Nakar, E., & Granot, J. 2007, MNRAS, 380, 1744
Nousek, J. A., et al. 2006, ApJ, 642, 389
Panaitescu, A., & Kumar, P. 2000, ApJ, 543, 66
Pandey, S. B., et al. 2009, A&A, 504, 45
Pe'er, A., & Wijers, R. A. M. J. 2006, ApJ, 643, 1036
Pei, Y. C. 1992, ApJ, 395, 130
Peng, F., Königl, A., & Granot, J. 2005, ApJ, 626, 966
Piran, T., Sari, R., & Zou, Y.-C. 2009, MNRAS, 393, 1107

Price, P. A., et al. 2002, ApJ, 572, L51
Racusin, J. L., et al. 2008, Nature, 455, 183
Rhoads, J. E. 1999, ApJ, 525, 737
Sari, R., Piran, T., & Halpern, J. P. 1999, ApJ, 519, L17
Savaglio, S., Glazebrook, K., & Le Borgne, D. 2009, ApJ, 691, 182
Savaglio, S., et al. 2005, ApJ, 635, 260
Schlegel, D. J., Finkbeiner, D. P., & Davis, M. 1998, ApJ, 500, 525
Stanek, K. Z., et al. 2006, Acta Astron., 56, 333
Svensson, K. M., Levan, A. J., Tanvir, N. R., Fruchter, A. S., & Strolger, L.-G. 2010, MNRAS, 405, 57
Tanvir, N. R., Levan, A. J., Fruchter, A. S., Graham, J., Wiersema, K., & Rol, E. 2008a, GRB Coordinates Network, 7569, 1
Tanvir, N. R., Perley, D. A., Levan, A. J., Bloom, J. S., Fruchter, A. S., & Rol, E. 2008b, GRB Coordinates Network, 7621, 1
Vreeswijk, P., et al. 2008, GRB Coordinates Network, 7444, 1
Wiersema, K., et al. 2007, A&A, 464, 529
Willmer, C. N. A., et al. 2006, ApJ, 647, 853
Wozniak, P. R., Vestrand, W. T., Panaitescu, A. D., Wren, J. A., Davis, H. R., & White, R. R. 2009, ApJ, 691, 495
Zeh, A., Klose, S., & Hartmann, D. H. 2004, ApJ, 609, 952
Zou, Y.-C., Piran, T., & Sari, R. 2009, ApJ, 692, L92